Bioprinting 26 (2022) e00194

Contents lists available at ScienceDirect

Bioprinting

journal homepage: www.sciencedirect.com/journal/bioprinting

Laser Assisted Bioprinting of laminin on biodegradable PLGA substrates: Effect on neural stem cell adhesion and differentiation

Silvia Tortorella [a, b], Pierpaolo Greco [f, h, *], Francesco Valle [d], Marianna Barbalinardo [d], Giulia Foschi [d], Francesca Lugli [e], Marco Dallavalle [g], Francesco Zerbetto [e], Carlo Augusto Bortolotti [c], Fabio Biscarini [c, h]

[a] Institute of Experimental Endocrinology and Oncology "Gaetano Salvatore", CNR, Via S. Pansini 5, 80131, Naples, Italy
[b] Department of Industrial Chemistry Toso Montanari, University of Bologna, Viale Risorgimento 4, 40136, Bologna, Italy
[c] Dip. Scienze della Vita, Università di Modena e Reggio Emilia, Via Campi 103, I – 41125, Modena, Italy
[d] Consiglio Nazionale delle Ricerche (CNR), Istituto per lo Studio dei Materiali Nanostrutturati (ISMN) – Via Piero Gobetti 101, I - 40129, Bologna, Italy
[e] Dip. Chimica "G. Ciamician", Università di Bologna, V. F. Selmi 2, 40126, Bologna, Italy
[f] Sezione di Fisiologia. Dipartimento di Neuroscienze e Riabilitazione, Università di Ferrara, Via Fossato di Mortara 17, 44121 Ferrara, Italy
[g] Department of Epidemiology, Institute for Medical Information Processing, Biometry and Epidemiology, Medical Faculty, Ludwig-Maximilians-Universität München, Munich, Germany
[h] Center for Translational Neurophysiology - Istituto Italiano di Tecnologia, Via Fossato di Mortara 17-19, I-44100, Ferrara, Italy

ARTICLE INFO

Keywords:
Laser assisted bioprinting
Neuron differentiation
Laminin
Coarse grained cells modelling
Atomic force microscopy
Cell culture spatial statistics
Biodegradable scaffolds
Chemical cues

ABSTRACT

Laser Assisted Bioprinting (LAB) is recognized to be an enabling and versatile microfabrication technology for regenerative medicine and artificial tissue engineering. Current bioprinting concentrates on a layer-by-layer approach to print cells in consecutive stacks or nets, to recreate specialized tissue functions with a top-down approach. This synthering of proximal cells however reduces the long range correlation of tissue parenchyma and stroma given by natural development, as result of cells mobility and signaling. In this work, laminin, one of the main components of brain extracellular matrix is deposited by LAB on a biodegradable scaffold made of poly (lactic-co-glycolic acid) (PLGA), providing chemical cues for the adhesion and differentiation of neural stem cells NE-4C induced by retinoic acid. Surface roughness and LAB induced aggregates promote the initial adhesion of neuronal stem cells to the PLGA substrate and influence the formation of clusters and interconnection between them. The amount of laminin delivered inside the spot area may be controlled down to sub-monolayer coverage and a positive correlation between the laminin spots and soma of trafficking cells is demonstrated, also by computational modelling. Anisotropic orientation of neurite outgrowth is induced upon differentiation, up to 70% of processes protruding from stem cell clusters. The comparative analysis shows that the topological cue plays a major role in enhabling cluster formation on the scaffold, but the bioprinted laminin spots appear to be regulating the strength of connection between them, opening the way to control the functional morphology of artificial neural tissue constructs.

1. Introduction

Laser Assisted Bioprinting (LAB) is a LIFT (Laser induced Forward Transfer)-based technique [1] that allows printing of soluble materials by generating an unstable fluid micro-jet by means of a focused laser beam. LIFT has been successfully tailored to print biological material such as peptides, proteins, DNA [2] but also components of organic electronics (semiconductors) [3] and appears to be an ideal candidate for hybrid fabrication protocols involving biosensors and artificially generated tissues. Recent reports show how to generate chemical cues and surface functionalization on 3D printed parts providing structural support for artificial organ models [4] as well as laser methods employed to print artificial microvascular network or to induce regeneration in bone defects. Inkjet printing has been extensively used to generate pattern of biopolymers [5] and cells [6], with high processing speed and resolution, especially with piezoelectric actuation systems. With respect to 1 pL droplets generated by nozzle-based inkjet printing, laser assisted methods allow to increase miniaturization, with droplets

* Corresponding author. Sezione di Fisiologia. Dipartimento di Neuroscienze e Riabilitazione, Università di Ferrara, Via Fossato di Mortara 17, 44121 Ferrara, Italy
E-mail address: pierpaolo.greco@unife.it (P. Greco).

https://doi.org/10.1016/j.bprint.2022.e00194
Received 27 September 2021; Received in revised form 18 January 2022; Accepted 18 January 2022
Available online 21 January 2022

of 0.1 pL volume. Along with inkjet printing, extrusion and light projection, LAB represents an enabling tool to assemble complex artificial tissues by seeding directly human stem cells in scaffold for differentiation, as reported for 3D corneal stromal mimicking structures [7], or in situ printing of mesenchymal stromal cells [8] with different geometric configuration, to study the effect of cell positioning on bone regeneration process. Clear evidence of growing microvasculature were recorded after seeding endothelial cells along a design of capillary network, with stacks of collagen and vascular endothelial growth factor [9]. Laser micromachining has been also employed to fabricate agarose based microfluidic compartments, mimicking extra cellular matrix (ECM) for seeding neuroblasts and forming nerve bundles in the animal model [10, 11]. Besides regenerative medicine, LAB has been explored also in studies on cancer cells dynamics ex vivo, to assess infiltration in non-cancerous tissue [12]. Glioblastoma (GBM) represents one of the major diseases targeted, since ex-vivo studies on natural explants may help in gather statistical information on heterogenicity, together with information coming from miRNAs assays [13]. Tang and coworkers [14] recently published a thorough review on the use of bioprinting for studying the interaction between the blood brain barrier and the brain extracellular matrix, highlighting the current difficulties to obtain variable permeability in artificial models of brain barrier. Impaired permeability is involved in the silent infiltration of GBM stem cells and reduced effectiveness of some therapeutic compounds. The ECM in proximity of the microvascular network, often referred as the vascular basement membrane, contains type IV collagen and glycoproteins such as laminin, fibronectin, entactin and vitronectin. It has been demonstrated that the local density of integrin receptors regulates the dynamics of cell adhesive response [15]. Usually chemical cues in ECM induce plasticity in endogenous cells that are in the proximity of the injury, stimulate the differentiation of stem cells recruited from different sites [16] and appear to exert an effective but debated role on GBM invasiveness and proliferation [17]. Laminin is a large glycoprotein (~900 kDa), formed by a complex of three units, with a shape that resembles a flexible cross. It is largely present on the basal lamina of stem cells and interacts with their integrins, promoting neurite growth, repair and remyelination [18]. Because of its large size, it is difficult to obtain high surface densities of its deposits with the correct orientations for ligand-receptor interaction. Different functionalization protocols are based on the assumption that γ-chains monomers of laminin mimick ECM, with larger surface densities of patterning and improved binding to the surface [19,20]. Therefore, laminin or derived peptides appear to be interesting components to be deposited with LAB on artificial constructs or materials, to investigate the interaction of neural cells with such chemical cues. In addition, other types of coating with bio-recognition units can be used to promote neuron-like differentiation. Microcontact printing (mCP) of self-assembled monolayers, micro-injection molding in capillaries (MIMICs) and lithographically controlled wetting (LCW) and similar unconventional lithographies have proved to be versatile and effective methods for creating patterns of predetermined shape and position with micrometric spatial resolution and sub-micrometer feature size [21–23]. These approaches based on soft-lithography are straightforward for creating patterns of a given material. Their drawbacks concern the re-positioning of the elastomeric stamp on the substrate for creating multiple patterns, as well as the possibility to deposit materials locally in a single spot. These limitations can be overcome by LAB specifically developed to print functional proteins [24]. The final resolution of the printed droplets depends on many parameters, such as the thickness of the bio-ink layer coated onto the ribbon, the surface tension and the viscosity of the bio-ink, the wettability and hydrophobicity of the substrate, the laser power, the distance between the ribbon and the substrate [25]. The wettability and hydrophobicity of the substrate play a minor role in the process, thanks to momentum of the liquid droplet, given by the jet.

In vitro studies have shown that topographical patterns may guide the adhesion of cells and growth of neurites and axons [26]. Structuring the surface topography of the scaffold with arrays of parallel lines is widely used to orient the direction of the neurites growing in restricted environment [27]. The characteristic periodicity of the channels or grooves influences the growth of neurites along the structure direction [28]. However, the bioprinted topographical modulation is not sufficient per se to ensure a stable adhesion and the chemical cues appear to be necessary for specific cell types. Also materials designed specifically to host cells before adhesion, i.e. hydrogels [29], combine both biochemical and mechanical stimuli to achieve control on density and spreading.

Here we report the patterning of laminin arrays on biodegradable polymeric films of PLGA (poly(lactic-co-glycolic acid)) to study stem cell adhesion and subsequent differentiation into neurons. Atomic Force Microscopy (AFM) and Scanning Electron Microscopy (SEM) imaging, together with immunofluorescence assays were used to study and model the mechanism that governs cell positioning during adhesion and neurite outgrowth during the differentiation phase. Simulations of cell adhesion onto material surfaces based on a coarse-grained model guided the choice of the optimal pattern geometry and helped to elucidate the cellular organization.

2. Materials and methods

2.1. Bioink-ribbon preparation

The laminin stock solution (500 μg/ml, Roche 11243217001 from mouse Engelbreth-Holm-Swarm (EHS) sarcoma, Purity: ≥ 90% SDS-PAGE as laminin-nidogen complex, 1:1) is diluted first in bi-distilled water and then in glycerol 1:2 to a final protein concentration of 15 μg/ml, and up to 150 μg/ml. The metal films on the ribbons were supplied by Organic Spintronics s.r.l., Bologna (Italy) and consist in glass slides coated by Pulsed Plasma Deposition (PPD) with a stainless steel layer (thickness = 20 nm). The ribbons were cleaned in Ethanol 99,9% (15 min sonication) and then gently dried in nitrogen flow. Laminin stock solution is diluted first in bi-distilled water and then in glycerol 1:2 (volume) to prepare the bioink with the final chosen protein concentration. Before the deposition of the bioink, each ribbon was placed in an oxygen plasma chamber (5', 30 mA) in order to make the surface more hydrophilic and suitable for spin-coating of the target solution. An aliquot of 400 μL of the bioink solution was spin coated at 1500 rpm onto the metallic layer of the ribbon forming a film of about 10 μm in thickness. Finally the ribbon was placed over the receiving substrate, using two PDMS spacers (approximate height = 600 μm).

2.2. Substrate preparation

PLGA was purchased from Sigma Aldrich (P1941, lactide:glycolide (75:25), mol wt 66000–107000). PLGA film (thickness = 20 μm) was prepared by solution casting using 5%wt of PLGA chloroform solution onto a cleaned glass substrate in a confining elastomeric frame (1.2 cm × 1.2 cm) or onto cleaned circular coverslips (≈1 cm). The glass slides, the coverslips and the elastomeric confining frames were cleaned with sonication in ethanol and allowed to dry. Then the frames were mounted on the glass surfaces taking care to make them adhering to each other. Once the PLGA was completely dissolved in chloroform, the liquid solution was poured onto the glass slides. After the complete evaporation of chloroform (5h in oven 37 °C), the frame was removed and the resulting transparent film was disinfected before use, by immersion in ethanol-water mixture (70:30).

Samples of PLGA scaffolds were further processed to obtain substrates with controlled roughness.

To obtain hydration of the scaffold and make it suitable for cell culture, PLGA has been incubated in D8537 Merck Dulbecco's Phosphate Buffered Saline 0.1x, for 24 h at 37 °C. After incubation the PLGA film was rinsed in deionized water. To obtain scaffolds with chemical cues, the non-hydrated PLGA thin film was used as substrate for LAB.

The two protocols have been performed as consecutive steps in order to achieve a scaffold with both high surface roughness and chemical cues. The films were incubated with PBS buffer for 24 h before the corrugated thin film was patterned with micro-droplets of laminin. LAB allows one to pattern biomolecules on substrates with large roughness, since the drop impacts the substrate with high kinetic energy, overcoming the resistance to wetting induced by increased roughness.

2.3. Laser Assisted Bioprinting

The optical setup developed in house for Laser Assisted Bioprinting is depicted in Fig. 1 The laser source is a solid Nd:YAG crystal laser (1064 nm wavelength, with 10ns pulse duration, frequency in a range of 5–50 KHz, variable driving voltage leading to peak power between 200 mW to and 1 W) and a precision motor stage for an accurate positioning of the samples. As specified in previous section the ribbon was coupled with the receiving poly(lactic-co-glycolic acid) (PLGA) substrate by means of two elastomeric supports, keeping a gap of 600 μm between the corresponding facing surfaces.

2.4. Cell culture

Investigation of stem cell line NE-4C interaction with the patterned substrate was carried out according to published cell culture protocols [21]. In brief, the stem cells were seeded at 25000 cells per cm^2 in a final volume of 400 mL of the complete medium (CM) (MEM containing 10% FBS, 4 mM glutamine, 40 mg/ml, 1 gentamicin and 2.5 mg/ml, 1 amphotericin) and incubated under the standard cell culture conditions (37C, 5% CO2 and 95% relative humidity). The test was repeated 3 times with 4 replicates upon PLGA substrates carrying LAB patterns of laminin (50 μg/ml, incubated overnight) with different periodicity between the spots, as reported in Fig. 4. Cell counting was performed with video microscopy, optical fluorescence imaging and SEM, averaging the number of cells and normalizing to optical image dimensions.

Cell differentiation experiment was repeated 4 times in 4 replicate wells, containing the PLGA substrates patterned with LAB. The laminin concentration in the bioink was 50 μg/ml, the spots periodicity has been kept equal to 50 μm, along the main axis of the pattern, and 100 μm between the lines of droplets (see inset in Fig. 6a). The LAB pattern was incubated overnight. Differentiation was induced by replacing CM, after 3 h, with the differentiation medium composed of DMEM-F12 Ham (1:1), ITS 1X, 4 mM glutamine, 40 μg/ml gentamicin and 2.5 μg/ml amphotericin (DM), containing all-trans retinoic acid (RA) 1 μM, according to protocol already reported in literature. After 2 days, the DM was replaced by DM containing 40 ng ml-1 brain-derived neurothropic factor (BDNF). Half of the DM was then changed every subsequent day by replacing it with DM, without any inducers until the end of experiment.

2.5. Immunostaining

Immunofluorescence of actin cytoskeleton and focal adhesions was performed with the Millipore staining kit (FAK 100), that contains fluorescent-labelled Phalloidin (TRITC-conjugated Phalloidin) and a monoclonal antibody to Vinculin to map the local orientation of actin filaments within the cell. DAPI staining for the fluorescent labelling of nuclei was carried out simultaneously.

To detect the effect of combined topographical and chemical cues, we investigated the adhesion of Ne-4C cultured on PLGA scaffolds patterned with LAB, in serum-free conditions. Immunofluorescence against adhesion proteins (Vinculin and Phalloidin) and nucleus (DAPI) revealed the presence and the position of neural stem cells, with respect to the PLGA scaffold and LAB array of laminin.

Immunofluorescence staining of β-Tubulin III, a neural differentiation marker, was performed co-labelling the nuclei with DAPI [19]. All the images were captured using an epifluorescence microscope (Nikon Eclipse 80i) endowed with NIKON excitation band DAPI-FITC-TRITC filter set and equipped with a digital camera (Nikon-DS-Fi1).

Laminin presence was also verified with immunofluorescence assay on PLGA as shown in Fig. 1c, Immunofluorescence assays were performed using a specific anti-laminin primary antibody (Sigma Aldrich L9393) and a secondary fluorescent antibody (AlexaFluor 594 Goat Anti-Rabbit IgG, Invitrogen A11012). Bioprinted laminin samples were blocked for 30 min with phosphate buffer saline (PBS) 1X containing 1% bovine serum albumin (blocking solution). They were incubated 1h at room temperature with antilaminin antibody diluted 1:25 in blocking solution, washed three times with PBS 1X, and incubated for 90 min at room temperature with the fluorescent Alexa Fluor 594 anti-rabbit antibody diluted 1:200 in PBS 1X. Immunoassay for laminin after cell seeding was not performed because of the red-signal of Phalloidin or Beta-Tubulin III was interfering on the analysis, and potentially leading to misinterpretation of results.

The morphology of the cells was monitored with optical microscopy (Nikon Eclipse 80i) at different times of incubation. Samples of differentiated cells were analyzed by Scanning Electron Microscopy (SEM). For SEM sample preparation, the cells were fixed with 2.5% glutaraldehyde (1 h; 4 °C) and post-fixed with 1% osmium tetroxide (1 h; r.t.), and then dehydrated in an increasing series of ethanol concentrations.

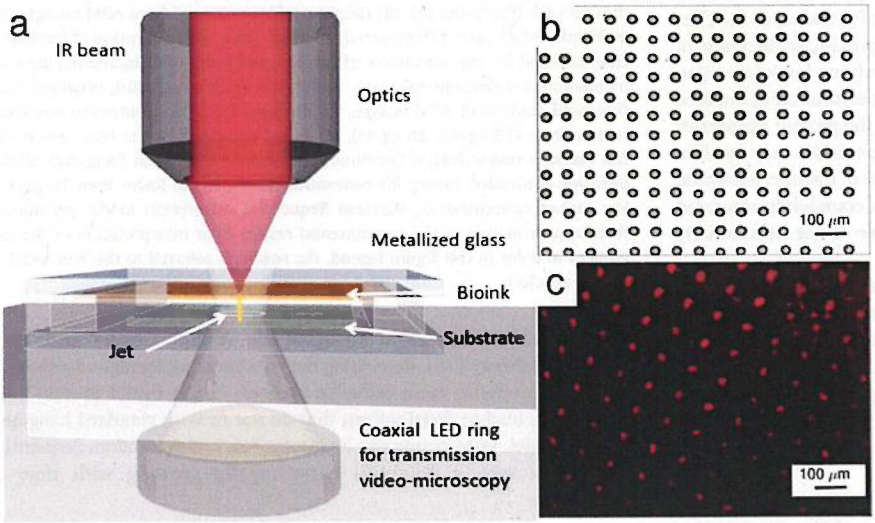

Fig. 1. ScribaR Multifunctional Laser Marker optical setup. The laser beam remains focused on the same plane, while the sample holder is translated along x and y axis according to imported design file. Pre-existing structures on the sample can be aligned to the LAB pattern using a coaxial videomicroscopy. (b) Optical microscopy images in bright field (10X) of bioprinted droplets printed with a center to center distance equal approximately to 50 μm. (c) Immunofluorescence assay shows the presence of laminin in each droplet deposited on the PLGA scaffold.

Subsequently, a gold thin film coating (10 nm) was sputtered before analysis with a SEM-FEG Hitachi S4000.

2.6. Spatial statistics

2.6.1. Correlation between laminin droplets and cells

The spatial correlation between the position of laminin droplets and cells for the different array periodicities was evaluated also with statistical software package *spatstat* [30]. Two sets of marked entities (points) [31] were associated to laminin spots (i) and cells (j) in SEM images with area of approximately 0.16 mm^2. The 2-dimensional coordinates of the center of each point entity with corresponding mark were recorded in file for computing the spatial correlation. The values of the characteristic probability function *markconnect* were recorded for each SEM image and further processed to calculate the correlation plot in Fig. 5b. Further detail and SEM images are reported in the Supporting Materials.

2.6.2. Neurite alignment

Alignment of neurites has been assessed starting from SEM images on cells cultivated for 11 days from the beginning of differentiation protocol. These neurites have been tracked using NeuronJ software [32], as a plugin of image analysis software ImageJ. The orientation of the line joining the starting and final points was classified according to the main direction of the pattern of adhesion protein, with histograms in polar coordinates, that report in color scale the length of analyzed neurites. The analysis of alignment was performed with package circular of statistics software R, in order to compare the distribution of neurites with circular uniform distribution. Several tests were applied to the vectors containing the sampled angles.

Further details on neurites alignment algorithm and computational model employed to analyse cells adhesion are provided in the Supplementary Materials.

3. Results

The chemical functionalization of the PLGA scaffold was studied by patterning several arrays of micro-droplets, starting from different initial concentration of laminin (15, 25, 50 μg/ml) and incubating the substrates for 30, 60, 120, and 240 min. The size of the spots of laminin after incubation does not depend on the concentration of the protein in the starting solution.

The AFM images in Fig. 2 show that laminin adsorbs on the substrate within the footprint of the micro-droplet, even for 15 μg/ml protein concentration. After 30 min of incubation, a partial monolayer of laminin appears, which does not entirely cover the area of the droplet. After 60 min of incubation, it is already noticeable the formation of 3D clusters on the surface. These aggregates have an approximate thickness of 40 nm and are randomly distributed on the underlying laminin carpet. After 120 min of incubation the coverage reaches saturation in the area occupied by the micro-droplet and it appears that the protein aggregates are weakly bound to the surface, as the washing operations may result in the displacement of protein outside of the footprint of the micro-droplet. At 240 min, the footprint of the micro-droplet is completely saturated with laminin, but the amount of protein available is not substantially different from 120 min of incubation.

It is important to mention that the laser assisted bioprinted droplet contains less than 0.05 pl of water, and the consequent degradation by hydrolysis of PLGA is almost negligible compared to the size of the scaffold employed in the experiment. The analysis of surface topography from AFM profiles (Fig. 2d) confirms that the degradation for LAB patterns is negligible compared to surface roughening occurring during hydration of the PLGA film in contact with a large volume of PBS buffer (Fig. 2c).

Fig. 2e shows the trend of AFM coverage, varying the initial concentration and time of incubation. The evolution of the coverage for

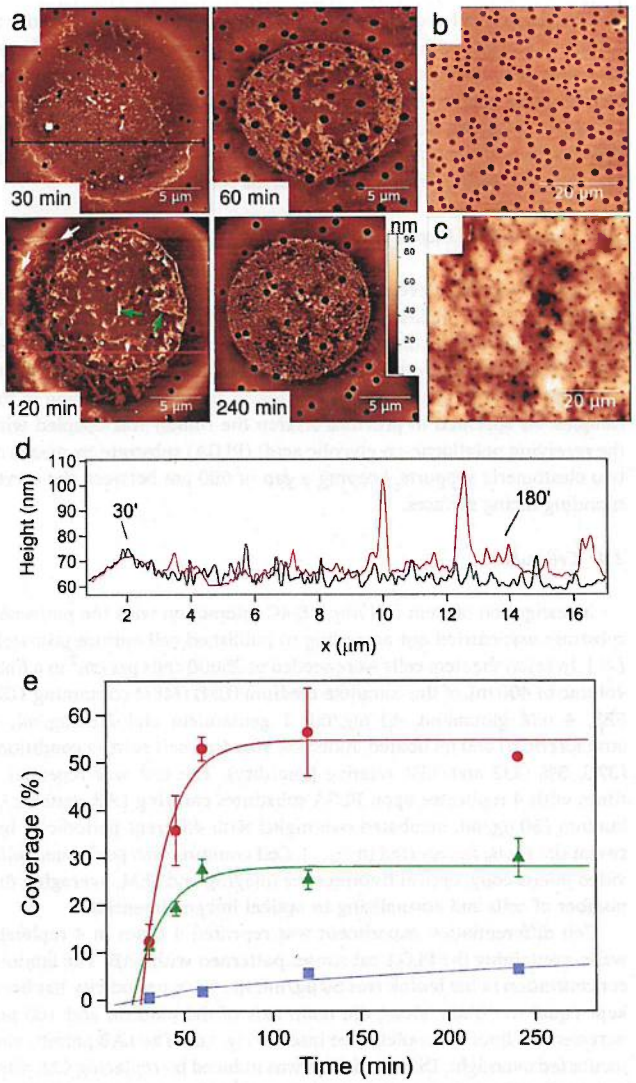

Fig. 2. (a) Laser Assisted Bioprinting of laminin on PLGA scaffold. AFM images taken at different incubation times. The white arrows indicate the protein aggregates weakly bound and displaced by the washing step. The green arrows show the beginning of a second layer of adsorbed protein. PLGA substrate used for neurite growth in differentiation study in pristine form (b) and after hydration with PBS buffer (c). (d) Height profiles extracted from AFM topography at 30 min (black) and 120 min (red) of incubation. The adsorption of laminin is characterized by the formation of larger aggregates with increasing time of incubation. (e) Laminin coverage, within the droplet footprint, obtained after threshold analysis of AFM images, for different initial concentration and incubation times (15 μg/ml, 25 μg/ml, 50 μg/ml corresponding to blue, green and red markers respectively). Continuous lines are fitting with Lang and Coates diffusion-controlled theory for concentration of protein lower than 15 μg/ml. For higher concentration, Random Sequential Adsorption model provides a finer approximation of the experimental results. (For interpretation of the references to color in this figure legend, the reader is referred to the Web version of this article.)

dilute concentrations below 15 μg/ml can be approximated with Lang and Coates theory [33], describing the number of molecules adsorbed on the surface upon a mere diffusive process. Larger initial protein concentrations lead to distributions that do not fit with standard Lang and Coates model. Data points can be interpolated with Random Sequential Adsorption with a sigmoidal curve rapidly growing with time of incubation.

3.1. Spatial distribution of NE-4C cells on the laminin pattern

The presence of NE-4C cells on the functional bioprinted scaffold has been assessed qualitatively with optical microscopy at 5 h from seeding. The shape of the cells confirmed the viability of proliferating cells on top of the PLGA film.

After 24 h, the number of adhered cells diminished substantially on the empty area of the PLGA scaffold, which was not functionalized with LAB, and eventually a large percentage detached from the substrates. The difference in cell density calculated after 24h of culturing between the functionalized area compared to the area without laminin bioprinting was substantial. These two values are $8.55 \times 10^4 \pm 1.29 \times 10^4$ cells/cm^2 and $1.12 \times 10^4 \pm 0.77 \times 10^4$ cell/cm^2, extracted from the optical fluorescence images and from SEM images [34]. The soma is extended across the smooth scaffold and the processes start to develop following the spots of laminin deposited by laser assisted bioprinting. A magnification of stem cells adhering on the functionalized PLGA is resolved in the immunofluorescence image in Fig. 3(c,d), whereas the correspondent positioning between cells and the bioprinted pattern can be spotted from the SEM images acquired after 24 h of culture. In Fig. 3 (b,f) it is possible to observe the shallow concavity of the micro-droplet footprint, left by the evaporation of the glycerol-water mixture. The ridge of the concavity seems to attract the stem cells, and it may be considered a slight topographic feature.

To confirm that neural stem cells are chemo-attracted, we performed the control experiment with PLGA thin scaffold, functionalized with laminin droplets on half of the culture plate. After the evaporation of glycerol, the substrates were put in culture with NE-4C and monitored at precise time intervals. The cells adhered most promptly on the area containing the laminin droplets, and almost none on the half of the PLGA surface of the same sample.

3.2. Simulations

The periodicity of the LAB pattern controls the probability of achieving a statistical matching between the LAB spots of laminin and the seeded neural stem cells. In Fig. 4a the cells adhering to PLGA with different periodic LAB arrays of laminin (40, 70, 100 μm) exhibit a decreasing tendency to follow the chemical cue during the adhesion phase. Simulations of single cell adhesion onto chemically patterned surfaces, based on a coarse-grained model, were carried out in order to select the optimal pattern geometry for the NE-4C differentiation experiments. Details of the model and of the simulation setup are described elsewhere [35] and in the Supplementary Materials. The adhesion probability (P) of a cell with a diameter of 15 μm was studied as a function of the pattern size, d, expressed as the distance between the centers of laminin droplets with a size of 20 μm. The probability of matching of a single cell with a laminin spot was estimated by running 100 statistically independent simulations where the cell is initially randomly placed on the surface and then is allowed to walk for a time. If the cell eventually reaches the droplet, which has a favourable interaction with cell, it stops on the laminin spot; otherwise, the cell does not adhere and eventually detaches from the surface (Fig. 4b). The matching probability is calculated as a function of simulation time (τ) for the three pattern geometries. The calculations showed that the probability, P, of cell-spot matching decreases with the increase of the droplet distance. For the pattern with d = 40 μm, at the end of the simulation time, it reaches almost the maximum possible value of P = 0.99, for d = 70 μm the value of P lowers to 0.46 and for d = 100 μm P is 0.21 (Fig. 4c). These results are in good agreement with experimental observations. Experimentally, the droplet pattern characterized by a distance between the spots of 40–70 μm yields a cell distribution that is effectively correlated with the LAB pattern. In the absence of chemical cue pattern, cells adhere onto the surface but form large clumps.

Radial power spectrum densities (RPSD) extracted from optical

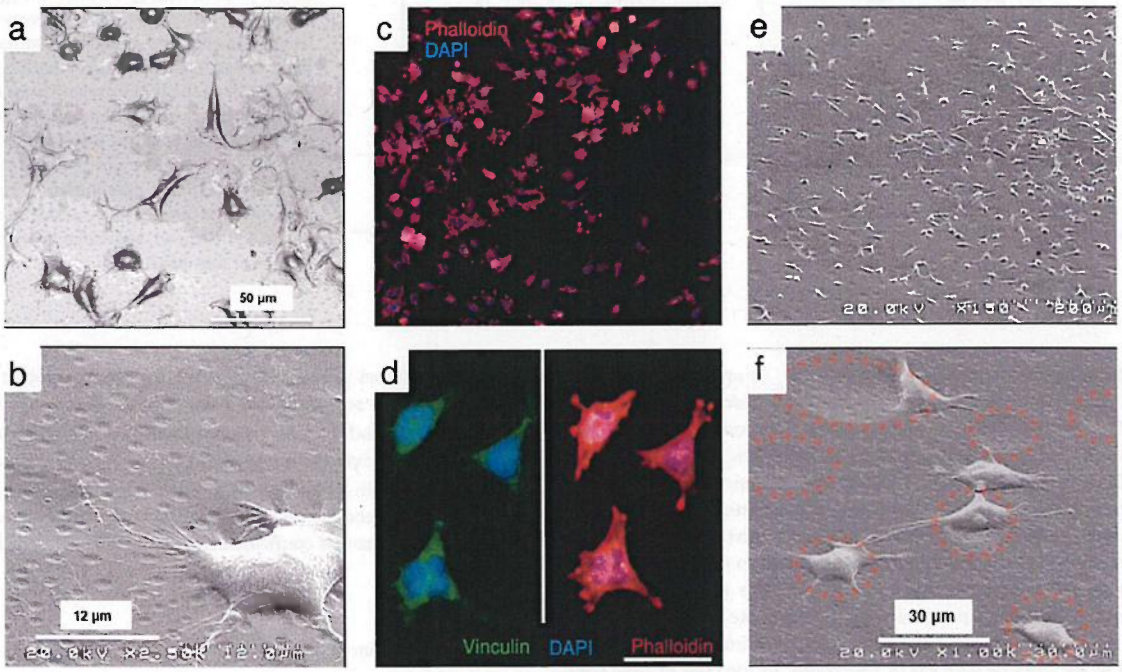

Fig. 3. Adhesion of NE-4C cells on pattern of laminin spots obtained with LAB: (a) Interference contrast image of NE-4C cell culture after 5 h from seed on PLGA substrate, (b) Detailed SEM magnification of cell soma sitting on top of laminin spot (c) Immunofluorescence of cell culture in proliferating medium condition after 24h from seeding (Phalloidin in red, merged with DAPI blue staining for the nuclei); (d) Magnification of stained cells localized on laminin pattern as in *b*. (Vinculin in green, Phalloidin in red, merged with DAPI blue staining for nuclei) Scale bar is 50 μm; (e) SEM image of stem cells adhering on PLGA scaffold patterned with laminin spots; (f) Enlarged detail showing stem cells extended over the border of the concavities left by evaporation of laminin solution from LAB-deposited droplets. Scale bar is 30 μm. (For interpretation of the references to color in this figure legend, the reader is referred to the Web version of this article.)

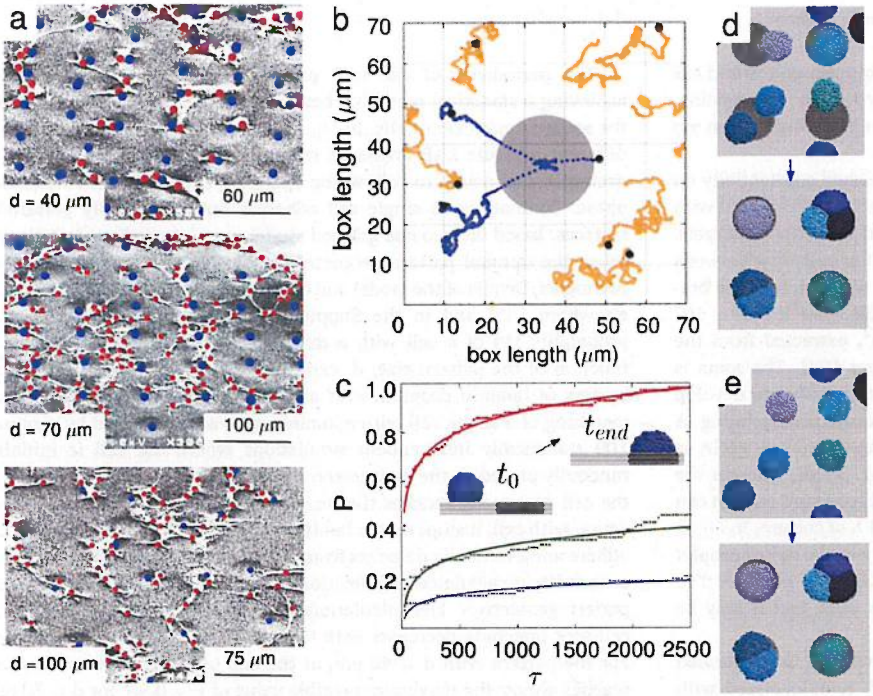

Fig. 4. a) SEM images with enhanced contrast of cells (red spots) adhering to a PLGA scaffold with laminin spots (blue spots) patterned with a mean periodicity of 40, 70 and 100 μm; (b) Coarse-grained simulations of cell adhesion onto the PLGA surface (black point is the initial position of the center of mass), the trajectories are represented according to effective reaching of the more adhesive region (blue trajectories will encounter the dark grey adhesive spot; orange trajectories will not); (c) the probability of encounter decreases with the distance between the adhesive spots: probability as a function of the simulation time for d = 40 (red), d = 70 (green) and d = 100 (blue) μm. In (b,c) the evolution in time during coarse-grained simulation is represented using the following color code: the cells (blue beads) are located on top of a planar solid surface (light grey beads) in the presence of a laminin spot (dark grey beads). Simulations of multiple cells adhesion onto LAB patterned PLGA scaffolds (d) and onto control surface (non patterned) (e). (For interpretation of the references to color in this figure legend, the reader is referred to the Web version of this article.)

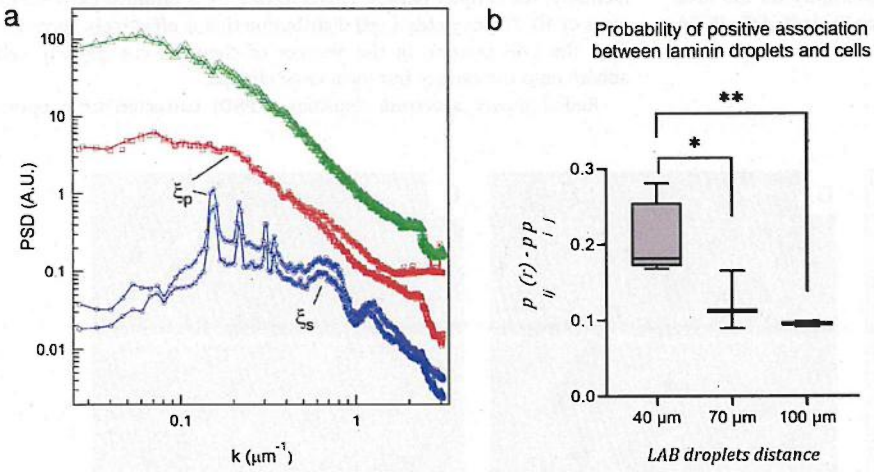

Fig. 5. (a) Comparison of power spectrum density of the images taken after deposition of laminin droplets and after immunostaining (blue circles for PSD of LAB pattern of laminin, red squares for PSD of cells adhered on LAB pattern, green triangles for PSD of cells adhered on plain PLGA scaffold). The correlation length pointed with ξ_p accounts for periodicity characteristic of the droplet array, whereas the correlation length termed ξ_s arises from the statistical diameter of the droplets. The correlation length ξ_p can be appreciated also on the PSD extracted from thresholding of fluorescence image. (b) Spatial correlation probability estimates for the three periodicities in LAB laminin arrays. $p_{ij}(r) - p_i p_j$ accounts for a positive association between the spatial distribution of laminin droplets and cells. (For interpretation of the references to color in this figure legend, the reader is referred to the Web version of this article.)

images (fluorescence) images is reported in Fig. 5a and compared with the RPSD of micro-droplets array. Fast Fourier transforms evidence the characteristic length scales of spatial correlations on the images. The wave vector k (μm-1) can be reported to characteristic length ξ, noticing that $\xi = 2\pi/k$. The RPSD curve of LAB shows evident peaks at low frequency, correspondent to the periodicity of the pattern ξ_p equal to 40 μm. A broader peak can be observed for characteristic length ξ_s equal approximately to 10 μm, which may be attributed to the average of the diameters of micro-droplets, considering also the satellite droplets, which may develop during patterning on hydrophobic substrates such as PLGA. In the same graph the RPSD plots calculated from cells image are compared to the ones of bare PLGA substrates. In the case of cells (red makers in Fig. 5a), it is possible to infer a change in the power fit at a frequency corresponding to 40 μm characteristic length scale.

Spatial statistics analysis based on 2D correlation of the geometric centers of laminin spots (i) and cells (j) is provided synthetically in Fig. 5b, for the three array periodicities. The probability $p_{ij}(r)$ is defined as the conditional probability that there exist two points belonging to different groups separated by a distance r. If we define $p_i p_j$ as the probability of random, independent distribution of the two point sets, the more $p_{ij}(r)$ deviates from $p_i p_j$ the more likely is the correlation between the laminin spots and cells. At distance of 40 μm, the positive association between the two sets is significantly larger than in the case of 70 and 100 μm case, as confirmed also in the diffusive particle dynamics simulation.

3.3. Differentiation of NE-4C

To investigate the competitive effect of morphological and chemical cues on differentiation of neural stem cells, PLGA substrates were prepared and incubated with 0.1x PBS buffer solution, in order to achieve a partial modification of surface morphology. The AFM images show a rough surface morphology (rms 60 nm) with superimposed textures of

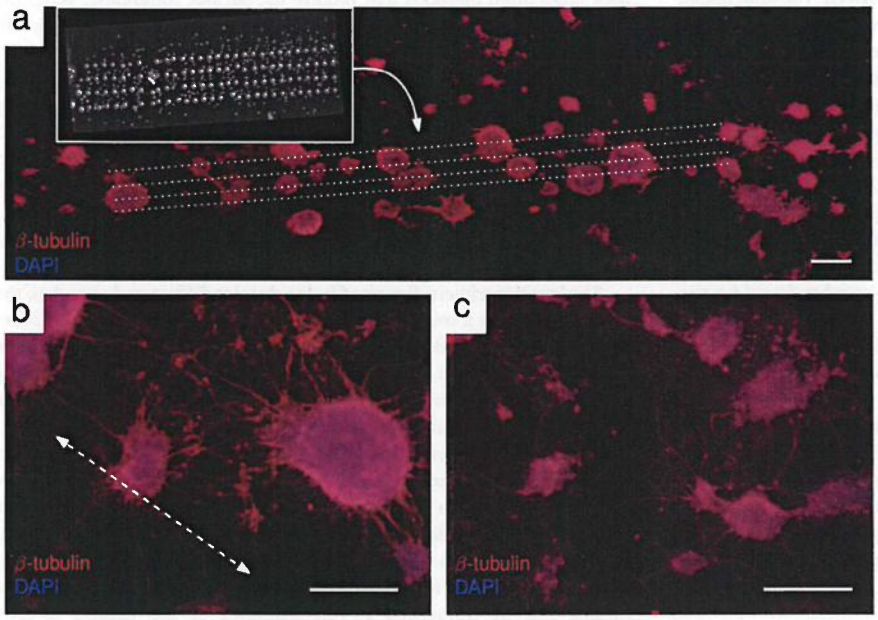

Fig. 6. Differentiation of NE-4C upon biodegradable PLGA scaffold, with topographical and chemical cues. (a) Immunofluorescence staining after 8 days from seeding. The configuration of the samples sees the superimposition of laminin droplets on a hydrated PLGA scaffold. The inset reports optical microscopy (dark-field) of the droplets with laminin after LAB patterning. (b) Detailed view of the neural processes, where a peculiar anisotropy may be appreciated in correlation with the droplets array. Dashed lines indicate the direction of the LAB pattern under neural clusters. (c) In the control sample, a reduced number of neurites are extending from cell clusters without preferential orientation. Scale bars are 100 μm.

small pores, characteristic of pristine PLGA (see Fig. 2b–c).

After PBS incubation, the PLGA scaffolds were patterned by LAB deposition of laminin droplets with a periodicity of 50 μm. In this manner, the neuronal stem cells felt either the topographical motives induced by increased roughness or both the topographical and chemical cues on the substrates. A couple of days after retinoic acid addition, the stem cells differentiated and started forming the initial connections that later developed into neural networks. Large circular clusters of interconnected cells developed on the PLGA scaffold with large roughness (see Fig. 6). During differentiation the NE-4C stem cells synthetize laminin directly, therefore the role of the chemical cue on the patterned substrates is mainly effective in the initial phase of cluster formation. The growth of cell aggregates appears to be three-dimensional, with neuron precursors extending from the boundaries of the clusters.

In Fig. 7a, two large aggregates, composed of hundreds of cells, adhere on PLGA functionalized with laminin. The neurites, protruding

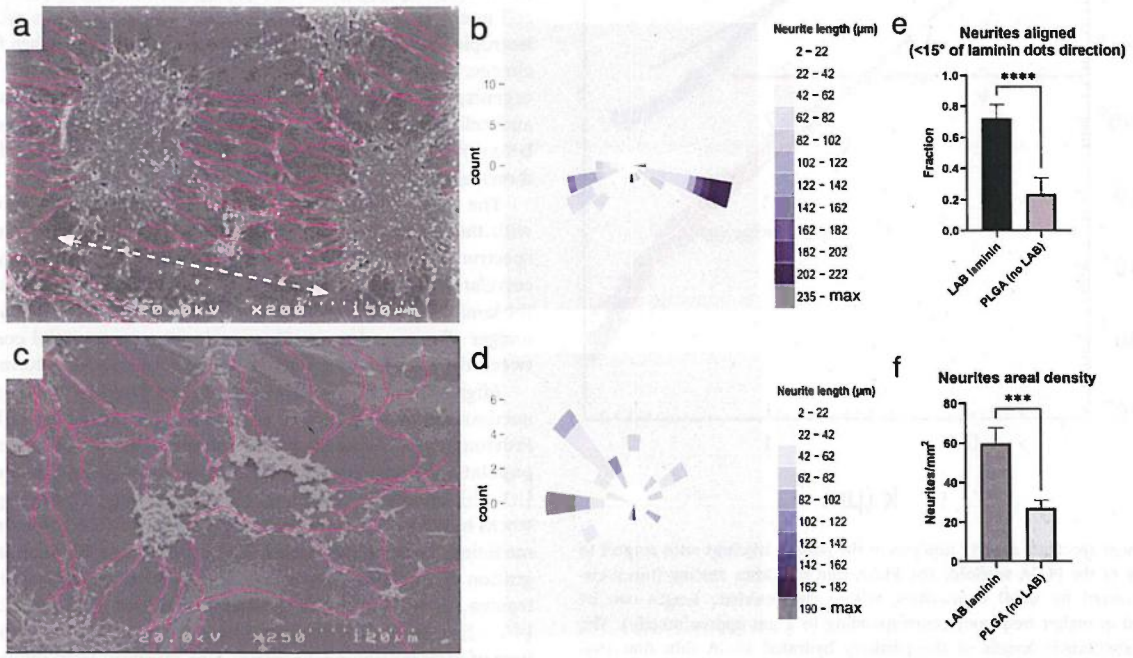

Fig. 7. (a) SEM images of neurites alignment. The arrow indicates the LAB pattern direction. The neurite processes are highlighted in violet; (b) Windrose plot showing the orientation of traced neurites. The color scale represents the length of neural processes; (c) The SEM image of the control sample, without LAB pattern, confirms the isotropic orientation; (d) of the neural processes when cells grow on substrates without chemical cues.(e) The fraction of neurites aligned within 15° of the main axis of the laminin pattern (see inset in Fig. 6a) is plot for the cell aggregates differentiating on top of the LAB pattern and on PLGA substrate without chemical cues. The same comparison is averaged and plot for the areal density of neurites, without constrain on their extending direction (f). (For interpretation of the references to color in this figure legend, the reader is referred to the Web version of this article.)

from each aggregate, are oriented along the LAB pattern. The SEM image provides texture detail to fluorescence evidence reported in Fig. 6. This anisotropic feature is not present in the control experiment, where neural stem cells have been cultured in the absence of laminin (see Fig. 6c). A larger set of images of interconnected network is provided in the Supplementary21 Materials. The percentage of neurites aligned within 15° of the main direction of the laminin spots pattern is reported in Fig. 7e. The LAB pattern induces a preferential alignment on more than 70% of the processes, whereas in the areas far from the LAB pattern, the distribution of processes appears to be isotropic. The surface density of neurites is also higher in the area above the LAB pattern, approximately 60 per mm^2 (Fig. 7f), almost doubling the number found for the PLGA substrate without the LAB pattern.

The PSD comparison between the PLGA scaffold (as cast), the hydrated PLGA scaffold and the neurites morphology, obtained after thresholding of SEM images, is reported in Fig. 8. In both PLGA substrates, it is evident the characteristic peak at higher frequencies relative to the pore size (≈2 μm). Moreover, the hydrated PLGA scaffold shows features at lower frequencies, due to the characteristic waviness of approximately 20 μm. This correlation length can be observed in the power spectrum extracted from the neurite tracings, suggesting that the morphology of neuronal processes follow the undulations of the hydrated PLGA scaffolds.

4. Discussion

Previous reports on the alignment induced by microstructures fabricated on scaffolds are based on a strict spatial correlation between the topographical features and chemical cues (i.e. laminin stripes). In cases where the topographic element, favouring cell growth, is obtained

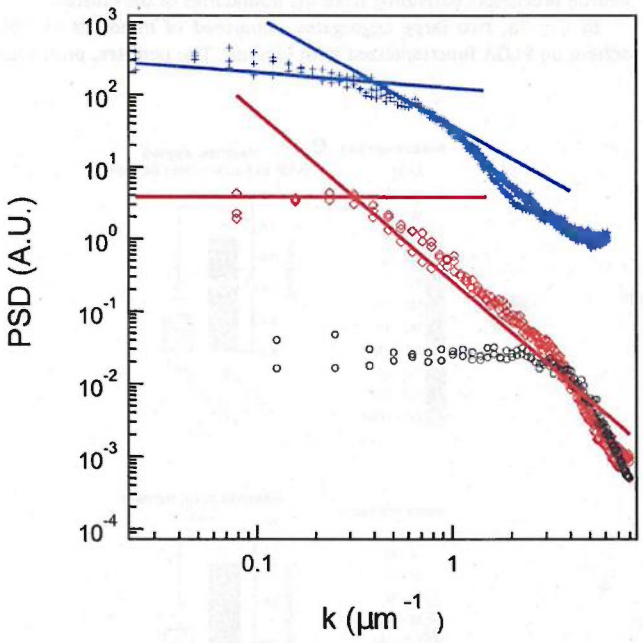

Fig. 8. Power spectrum density analysis of the neurite tracings with respect to topography of the PLGA scaffold. The PLGA thin film after casting (black circles) is covered by small concavities, whose characteristic length can be appreciated at higher frequency (corresponding to 2 μm approximately). The second characteristic length of the partially hydrated PLGA thin film (red rhombus) can be observed at lower frequency, corresponding to 20 μm approximately. The power spectra of the neurite images (blue cross) highlight a feature with the same correlation length. The spectra have been fitted with power law with different exponents (intersecting segments) to highlight the characteristic length of 20 μm. (For interpretation of the references to color in this figure legend, the reader is referred to the Web version of this article.)

with fabrication methods that modify the surface roughness, generally the chemical cue is made by a functionalization of the overall surface. In our case, we tried to separate the fabrication processes to make uncorrelated overlaps between topographic stimulus (surface with high roughness), and chemical functionalization. This was achieved by using an additive technique such as the laser assisted bioprinting. The LAB microjet deposits the laminin droplets upon a biodegradable scaffold (PLGA), which does not immediately absorb the excess of water-glycerol solution, therefore the laminin solution remains in incubation upon the surface for a defined period of time, before the complete evaporation of glycerol-water component, taking more than 24 h to complete.

The laminin trimers dispersed in the droplet diffuse and adsorb to the surface following a trend that may be interpreted with Lang and Coates theory [33], for initial concentration below 15 μg/ml. According to the proposed mechanism, the adsorption of biomolecules is effectively controlled just by the diffusion coefficient in solution because the interaction between molecules at the surface does not interfere with adsorption. The surface coverage and the morphology of the protein thin film may be controlled changing the time of incubation or the concentration of the protein within the bioink film. At concentration higher than 15 μg/ml, the film growth resembles random sequential adsorption, since aggregates with 3D structure are formed preserving the underlying monolayer. In this case, the laminin molecules reaching the surface will be influenced by the presence of the trimers already adsorbed on the scaffold, and will diffuse on the surface up to a certain path. This sequential mechanism is reported in literature to account for a Langmuir adsorption [36], which fits the reported coverage data, obtained by AFM.

During the cell adhesion experiment, the morphology of the PLGA surface was not significantly changed by LAB patterning, exception taken for the very shallow concavity resulting from evaporation of the water-glycerol. If we look at the correlations between the LAB pattern and the adhering cells, we can assess whether the laminin pattern is really influential for the placement of each cell. Cells seeded onto a homogeneous surface form unorganized clumps. In the absence of vicinal chemical cues, the cell adhesion onto the surface is driven by cell-cell interaction. It is reasonable to expect that neurites growth will be isotropic. Cells seeded onto a chemically patterned surface form smaller clusters placed on the laminin spots. Small cell clusters attach and organize on the same laminin spot, trying to optimize both cell-surface and cell-cell favourable interactions. If the distance between spots is between 40 and 70 μm, it is reasonable to expect that neurites growth is directional.

The optical fluorescence images immunostaining were compared with the droplets pattern immediately after deposition and the power spectrum densities (PSD) of the two images (Fig. 8) revealed that the correlation length ξ_p, relative to the mean statistical distance between the laminin droplets, can be observed also in the PSD calculated from the images of neuronal soma. This result suggests a spatial correlation between the laminin spots and the position of the cells, during adhesion.

Alignment of neurites has been investigated by looking at the connections between groups of stem cells that are facing differentiation. Previous works focused on the extension of neural processes from a population of primary neurons, in presence of geometrical confinement [37–39]. Exerting a control on the alignment of developing neural networks is interesting for potential applications in the field of regenerative medicine, because the patterning protocol can be exploited for integration of implants that favour regeneration of nervous tissues, after trauma, according to a geometry required for function recovery [40–42]. LAB of ECM components in layered constructs will be at the base of complex tissue fabrication, also cancer in-vitro models, to induce endothelial cells organization and microvascular generation as in glioblastoma artificial stroma [14].

The development of neural processes statistically oriented along the array of laminin droplets follows in time the growth of clusters of differentiated stem cells. The potential attraction exerted by the pattern

depends on the concentration of the adhesion proteins on the surface, which must exceed the one synthetized by the cells in surrounding of cellular membrane [43]. The results show the clear effect of the LAB pattern of laminin deposited on PLGA, on the growth of thicker neuronal processes along a preferential direction. From the applicative point of view, along the direction of the pattern we are able to build interconnected networks starting from initial seed of stem cells.

The alignment of neurites protruding from cell aggregates were compared with circular uniform distribution (Watson, Kuiper and Rayleigh) [42,44], and all the performed tests return statistics relevance for alignment. The percentage of neurites aligned according to the long axis of the pattern is larger than 70%, whereas the remaining part is still distributed in an isotropic way on the substrate and reflects the tendency of cell aggregates to look for chemical cues in every direction.

The results confirm that the neural stem cells are able to differentiate only on the areas where the morphology of PLGA yields a larger surface roughness. The laminin pattern, without an effective surface roughness, is not sufficient to achieve the proper environment for differentiation of neural cells' clusters. No evident neurites orientation could be obtained in this case.

5. Conclusions

The detailed description of the influence of micro and nanoscale roughness upon stem cell differentiation is still under debate [44]. Recent work has proposed a mechanism of selective differentiation by means of linear micropatterns [34], or nanometric ridge/groove arrays that induce differentiation of human embryonic stem cells into neurons [45,46]. However, most of the literature employ simultaneously a fabrication process to accomplish a topographical cue on the scaffold surface, and a functionalization process to anchor adhesion proteins or peptides over the topographical guidances.

In the present work, we performed fabrication and functionalization of biodegradable scaffolds, in order to decouple the two effects: the roughness increase of partially hydrated PLGA scaffold, and the functionalization, in specific areas, with adhesion protein laminin.

Laser Assisted Bioprinting is a new technology for patterning biodegradable scaffolds suitable in regenerative medicine. The capability to optically see through the LAB target, and align with the underlying substrates, in our opinion, represents a step forward in the microfabrication of implantable devices for nerve regeneration and cancer research. Within the described experiments, LAB was applied to pattern arrays of laminin droplets upon PLGA scaffolds, with variable surface roughness. We found that neural stem cells adhere upon laminin pattern, also when PLGA had no topographic guidance. Differentiation, however, occurs only in presence of hydrated PLGA scaffolds, with roughness larger than 60 nm. The presence of laminin spots induced anisotropic orientation of the neurite processes extending out of large clusters of cells. The data interpretation was assisted by computer modelling of cell adhesion onto patterned surface. When the pattern of laminin is characterized by a distance between the spots of 40 μm, the probability of adhesion is close to 100%.

Exploitation of LAB microfabrication, to tailor the morphological and chemical cues for adhesion and differentiation, represent a valuable tool for studying the recruiting and differentiation of stem cells for regenerative medicine and for developing printed constructs to investigate the cellular path of diseases with innate heterogeneity.

CRediT authorship contribution statement

Silvia Tortorella: Investigation, Data curation, Methodology, Writing – original draft, Writing – review & editing. **Pierpaolo Greco:** Conceptualization, Data curation, Formal analysis, Supervision, Writing – original draft, Writing – review & editing. **Francesco Valle:** Data curation, Methodology, Supervision, Writing – review & editing. **Marianna Barbalinardo:** Data curation, Methodology, Supervision, Writing – review & editing. **Giulia Foschi:** Data curation, Methodology, Supervision, Writing – review & editing. **Francesca Lugli:** Computational chemistry model, Data curation, Formal analysis, Writing – review & editing. **Marco Dallavalle:** Computational chemistry model, Data curation, Formal analysis, Writing – review & editing. **Francesco Zerbetto:** Methodology, Validation, Supervision, Funding acquisition, Writing – review & editing. **Carlo Augusto Bortolotti:** Methodology, Validation, Supervision, Funding acquisition, Writing – review & editing. **Fabio Biscarini:** Conceptualization, Formal analysis, Modelling, Validation, Supervision, Funding acquisition, Writing – original draft, Writing – review & editing.

Declaration of competing interest

The authors declare that they have no known competing financial interests or personal relationships that could have appeared to influence the work reported in this paper.

Acknowledgments

This work was financially supported by the European Commission through the Marie Sklodowska-Curie ITN projects "BORGES" grant n. 813863, by the EuroNanoMed III project "AMI" and by the Life Science Department of the University of Modena and Reggio Emilia, through "FAR2018"

Appendix A. Supplementary data

Supplementary data to this article can be found online at https://doi.org/10.1016/j.bprint.2022.e00194.

References

[1] J. Bohandy, B.F. Kim, F.J. Adrian, Metal deposition from a supported metal film using an excimer laser, J. Appl. Phys. 60 (1986) 1538, https://doi.org/10.1063/1.337287.

[2] F. Guillemot, A. Souquet, S. Catros, B. Guillotin, J. Lopez, M. Faucon, B. Pippenger, R. Bareille, M. Rémy, S. Bellance, P. Chabassier, J.C. Fricain, J. Amédée, High-throughput laser printing of cells and biomaterials for tissue engineering, Acta Biomater. 6 (2010) 2494–2500, https://doi.org/10.1016/j.actbio.2009.09.029.

[3] L. Rapp, C. Constantinescu, P. Delaporte, A.P. Alloncle, Laser-induced forward transfer of polythiophene-based derivatives for fully polymeric thin film transistors, Org. Electron. 15 (2014) 1868–1875, https://doi.org/10.1016/j.orgel.2014.04.029.

[4] C. Dou, V. Perez, J. Qu, A. Tsin, B. Xu, J. Li, A State-Of-The-Art Review of Laser-Assisted Bioprinting and its Future Research Trends, ChemBioEng Reviews. n/a, 2021, https://doi.org/10.1002/cben.202000037.

[5] S. Ramasamy, P. Davoodi, S. Vijayavenkataraman, J.H. Teoh, A. M. Thamizhchelvan, K.S. Robinson, B. Wu, J.Y.H. Fuh, T. DiColandrea, H. Zhao, E. B. Lane, C.-H. Wang, Optimized construction of a full thickness human skin equivalent using 3D bioprinting and a PCL/collagen dermal scaffold, Bioprinting 21 (2021), e00123, https://doi.org/10.1016/j.bprint.2020.e00123.

[6] Y.C. Oztan, N. Nawafleh, Y. Zhou, P.Y. Liyanage, S.D. Hettiarachchi, E.S. Seven, R. M. Leblanc, A. Ouhtit, E. Celik, Recent advances on utilization of bioprinting for tumor modeling, Bioprinting 18 (2020), e00079, https://doi.org/10.1016/j.bprint.2020.e00079.

[7] A. Sorkio, L. Koch, L. Koivusalo, A. Deiwick, S. Miettinen, B. Chichkov, H. Skottman, Human stem cell based corneal tissue mimicking structures using laser-assisted 3D bioprinting and functional bioinks, Biomaterials 171 (2018) 57–71, https://doi.org/10.1016/j.biomaterials.2018.04.034.

[8] V. Keriquel, H. Oliveira, M. Rémy, S. Ziane, S. Delmond, B. Rousseau, S. Rey, S. Catros, J. Amédée, F. Guillemot, J.-C. Fricain, In situ printing of mesenchymal stromal cells, by laser-assisted bioprinting, for in vivo bone regeneration applications, Sci. Rep. 7 (2017) 1778, https://doi.org/10.1038/s41598-017-01914-x.

[9] O. Kérourédan, J.-M. Bourget, M. Rémy, S. Crauste-Manciet, J. Kalisky, S. Catros, N.B. Thébaud, R. Devillard, Micropatterning of endothelial cells to create a capillary-like network with defined architecture by laser-assisted bioprinting, J. Mater. Sci. Mater. Med. 30 (2019) 28, https://doi.org/10.1007/s10856-019-6230-1.

[10] A. Doraiswamy, T. Patz, R.J. Narayan, M. Dinescu, R. Modi, R.C.Y. Auyeung, D. B. Chrisey, Two-dimensional differential adherence of neuroblasts in laser micromachined CAD/CAM agarose channels, Appl. Surf. Sci. 252 (2006) 4748–4753, https://doi.org/10.1016/j.apsusc.2005.07.158.

[11] S. England, A. Rajaram, D.J. Schreyer, X. Chen, Bioprinted fibrin-factor XIII-hyaluronate hydrogel scaffolds with encapsulated Schwann cells and their in vitro

characterization for use in nerve regeneration, Bioprinting 5 (2017) 1–9, https://doi.org/10.1016/j.bprint.2016.12.001.
[12] T.B. Phamduy, R.S. Sweat, M.S. Azimi, M.E. Burow, W.L. Murfee, D.B. Chrisey, Printing cancer cells into intact microvascular networks: a model for investigating cancer cell dynamics during angiogenesis, Integrat. Biol. 7 (2015) 1068–1078, https://doi.org/10.1039/c5ib00151j.
[13] M. Selvaraj, P. Greco, M. Sensi, G.D. Saygin, N. Bellassai, R. D'Agata, G. Spoto, F. Biscarini, Label free detection of miRNA-21 with electrolyte gated organic field effect transistors (EGOFETs), Biosens. Bioelectron. 182 (2021) 113144, https://doi.org/10.1016/j.bios.2021.113144.
[14] M. Tang, J.N. Rich, S. Chen, Biomaterials and 3D bioprinting strategies to model glioblastoma and the blood–brain barrier, Adv. Mater. 33 (2021), https://doi.org/10.1002/adma.202004776, 2004776.
[15] E.A. Cavalcanti-Adam, T. Volberg, A. Micoulet, H. Kessler, B. Geiger, J.P. Spatz, Cell spreading and focal adhesion dynamics are regulated by spacing of integrin ligands, Biophys. J. 92 (2007) 2964–2974, https://doi.org/10.1529/biophysj.106.089730.
[16] F. Cimadamore, K. Fishwick, E. Giusto, K. Gnedeva, G. Cattarossi, A. Miller, S. Pluchino, L.M. Brill, M. Bronner-Fraser, A.V. Terskikh, Human ESC-derived neural crest model reveals a key role for SOX2 in sensory neurogenesis, Cell Stem Cell 8 (2011) 538–551, https://doi.org/10.1016/j.stem.2011.03.011.
[17] J.T. Gamble, Y. Reed-Harris, C.L. Barton, J. La Du, R. Tanguay, J.A. Greenwood, Quantification of glioblastoma progression in zebrafish xenografts: adhesion to laminin alpha 5 promotes glioblastoma microtumor formation and inhibits cell invasion, Biochem. Biophys. Res. Commun. 506 (2018) 833–839, https://doi.org/10.1016/j.bbrc.2018.10.076.
[18] W. Daly, L. Yao, D. Zeugolis, A. Windebank, A. Pandit, A biomaterials approach to peripheral nerve regeneration: bridging the peripheral nerve gap and enhancing functional recovery, J. R. Soc. Interface 9 (2012) 202–221, https://doi.org/10.1098/rsif.2011.0438.
[19] X. Chen, M.A. Brewer, C. Zou, P.J. Campagnola, Adhesion and migration of ovarian cancer cells on crosslinked laminin fibers nanofabricated by multiphoton excited photochemistry, Integr. Biol. 1 (2009) 469–476, https://doi.org/10.1039/B906310B.
[20] H.S. Koh, T. Yong, W.E. Teo, C.K. Chan, M.E. Puhaindran, T.C. Tan, A. Lim, B. H. Lim, S. Ramakrishna, In vivo study of novel nanofibrous intra-luminal guidance channels to promote nerve regeneration, J. Neural. Eng. 7 (2010), 046003, https://doi.org/10.1088/1741-2560/7/4/046003.
[21] B. Chelli, M. Barbalinardo, F. Valle, P. Greco, E. Bystrenova, M. Bianchi, F. Biscarini, Neural cell alignment by patterning gradients of the extracellular matrix protein laminin, Interface Focus 4 (2014) 20130041, https://doi.org/10.1098/rsfs.2013.0041.
[22] E. Ostuni, G.M. Whitesides, D.E. Ingber, C.S. Chen, Using self-assembled monolayers to pattern ECM proteins and cells on substrates, in: S. Even-Ram, V. Artym (Eds.), Extracellular Matrix Protocols, Humana Press, Totowa, NJ, 2009, pp. 183–194. http://www.springerprotocols.com/Abstract/doi/10.1007/978-1-59745-413-1_12. (Accessed 23 September 2013).
[23] M. Ventre, F. Valle, M. Bianchi, F. Biscarini, P.A. Netti, Cell fluidics: producing cellular streams on micropatterned synthetic surfaces, Langmuir 28 (2011) 714–721, https://doi.org/10.1021/la204144k.
[24] J.A. Barron, R. Rosen, J. Jones-Meehan, B.J. Spargo, S. Belkin, B.R. Ringeisen, Biological laser printing of genetically modified Escherichia coli for biosensor applications, Biosens. Bioelectron. 20 (2004) 246–252, https://doi.org/10.1016/j.bios.2004.01.011.
[25] M. Duocastella, M. Colina, J.M. Fernández-Pradas, P. Serra, J.L. Morenza, Study of the laser-induced forward transfer of liquids for laser bioprinting, Appl. Surf. Sci. 253 (2007) 7855–7859, https://doi.org/10.1016/j.apsusc.2007.02.097.
[26] L. Yao, S. Wang, W. Cui, R. Sherlock, C. O'Connell, G. Damodaran, A. Gorman, A. Windebank, A. Pandit, Effect of functionalized micropatterned PLGA on guided neurite growth, Acta Biomater. 5 (2009) 580–588, https://doi.org/10.1016/j.actbio.2008.09.002.
[27] H.N. Kim, A. Jiao, N.S. Hwang, M.S. Kim, D.H. Kang, D.-H. Kim, K.-Y. Suh, Nanotopography-guided tissue engineering and regenerative medicine, Adv. Drug Deliv. Rev. 65 (2013) 536–558, https://doi.org/10.1016/j.addr.2012.07.014.
[28] J. Xie, M.R. MacEwan, X. Li, S.E. Sakiyama-Elbert, Y. Xia, Neurite outgrowth on nanofiber scaffolds with different orders, structures, and surface properties, ACS Nano 3 (2009) 1151–1159, https://doi.org/10.1021/nn900070z.
[29] Q. Wei, J. Young, A. Holle, J. Li, K. Bieback, G. Inman, J.P. Spatz, E.A. Cavalcanti-Adam, Soft hydrogels for balancing cell proliferation and differentiation, ACS Biomater. Sci. Eng. 6 (2020) 4687–4701, https://doi.org/10.1021/acsbiomaterials.0c00854.
[30] Spatial Point Patterns: Methodology and Applications with R, Routledge & CRC Press. (n.d.). https://www.routledge.com/Spatial-Point-Patterns-Methodology-and-Applications-with-R/Baddeley-Rubak-Turner/p/book/9781482210200 (accessed January 8, 2022).
[31] Fractals, Random Shapes and Point Fields: Methods of Geometrical Statistics | Wiley, Wiley.Com. (n.d.). https://www.wiley.com/en-us/Fractals%2C+Random+Shapes+and+Point+Fields%3A+Methods+of+Geometrical+Statistics-p-9780471937579 (accessed January 9, 2022).
[32] E. Meijering, M. Jacob, J.-C. f. Sarria, P. Steiner, H. Hirling, M. Unser, Design and validation of a tool for neurite tracing and analysis in fluorescence microscopy images, Cytometry 58A (2004) 167–176, https://doi.org/10.1002/cyto.a.20022.
[33] D. Lang, P. Coates, Diffusion coefficient of DNA in solution at "zero" concentration as measured by electron microscopy, J. Mol. Biol. 36 (1968) 137–151.
[34] I. Tonazzini, E. Bystrenova, B. Chelli, P. Greco, P. Stoliar, A. Calò, A. Lazar, F. Borgatti, P. D'Angelo, C. Martini, F. Biscarini, Multiscale morphology of organic semiconductor thin films controls the adhesion and viability of human neural cells, Biophys. J. 98 (2010) 2804–2812, https://doi.org/10.1016/j.bpj.2010.03.036.
[35] M. Dallavalle, F. Lugli, S. Rapino, F. Zerbetto, "Active" drops as phantom models for living cells: a mesoscopic particle-based approach, Soft Matter 12 (2016) 3538–3544, https://doi.org/10.1039/C5SM02686E.
[36] M. Rabe, D. Verdes, S. Seeger, Understanding protein adsorption phenomena at solid surfaces, Adv. Colloid Interface Sci. 162 (2011) 87–106, https://doi.org/10.1016/j.cis.2010.12.007.
[37] K. Onuma, N. Kanzaki, Size distribution and intermolecular interaction of laminin-1 in physiological solutions, J. Phys. Chem. B 107 (2003) 11799–11804, https://doi.org/10.1021/jp0355298.
[38] J.M. Corey, D.Y. Lin, K.B. Mycek, Q. Chen, S. Samuel, E.L. Feldman, D.C. Martin, Aligned electrospun nanofibers specify the direction of dorsal root ganglia neurite growth, J. Biomed. Mater. Res. 83A (2007) 636–645, https://doi.org/10.1002/jbm.a.31285.
[39] F. Johansson, P. Carlberg, N. Danielsen, L. Montelius, M. Kanje, Axonal outgrowth on nano-imprinted patterns, Biomaterials 27 (2006) 1251–1258, https://doi.org/10.1016/j.biomaterials.2005.07.047.
[40] I. Tonazzini, S. Meucci, P. Faraci, F. Beltram, M. Cecchini, Neuronal differentiation on anisotropic substrates and the influence of nanotopographical noise on neurite contact guidance, Biomaterials 34 (2013) 6027–6036, https://doi.org/10.1016/j.biomaterials.2013.04.039.
[41] C. Cossetti, C. Alfaro-Cervello, M. Donegà, G. Tyzack, S. Pluchino, New perspectives of tissue remodelling with neural stem and progenitor cell-based therapies, Cell Tissue Res. 349 (2012) 321–329, https://doi.org/10.1007/s00441-012-1341-8.
[42] M. Cusimano, D. Biziato, E. Brambilla, M. Donegà, C. Alfaro-Cervello, S. Snider, G. Salani, F. Pucci, G. Comi, J.M. Garcia-Verdugo, M.D. Palma, G. Martino, S. Pluchino, Transplanted neural stem/precursor cells instruct phagocytes and reduce secondary tissue damage in the injured spinal cord, Brain 135 (2012) 447–460, https://doi.org/10.1093/brain/awr339.
[43] S.A. Ross, R.A. Ahrens, L.M. De Luca, Retinoic acid enhances adhesiveness, laminin and integrin β1 synthesis, and retinoic acid receptor expression in F9 teratocarcinoma cells, J. Cell. Physiol. 159 (1994) 263–273, https://doi.org/10.1002/jcp.1041590210.
[44] J.A. Mitchel, D. Hoffman-Kim, Cellular scale Anisotropic topography guides schwann cell motility, PLoS One 6 (2011), e24316, https://doi.org/10.1371/journal.pone.0024316.
[45] L. Qi, N. Li, R. Huang, Q. Song, L. Wang, Q. Zhang, R. Su, T. Kong, M. Tang, G. Cheng, The effects of topographical patterns and sizes on neural stem cell behavior, PLoS One 8 (2013), e59022, https://doi.org/10.1371/journal.pone.0059022.
[46] M.R. Lee, K.W. Kwon, H. Jung, H.N. Kim, K.Y. Suh, K. Kim, K.-S. Kim, Direct differentiation of human embryonic stem cells into selective neurons on nanoscale ridge/groove pattern arrays, Biomaterials 31 (2010) 4360–4366, https://doi.org/10.1016/j.biomaterials.2010.02.012.